Supplementary Information

Plasmon-Mediated Nonradiative Energy Transfer from Conjugated Polymer to a Plane of Graphene-Nanodot-Supported Silver Nanoparticles: An Insight into Characteristic Distance

Yunjing Wang,[§a] Hanmei Li,[§a] Weiwei Zhu,[a] Futao He,[a] Yongwei Huang,[b] Ruifeng Chong,[a] Dongxing Kou,[a] Wenkai Zhang,[*a] Xianrui Meng,[*a] Xiaomin Fang[*a]

[a]Institute of Fine Chemistry and Engineering, Henan Engineering Laboratory of Flame-Retardant and Functional Materials, College of Chemistry and Chemical Engineering, Henan University, Kaifeng 475004, P. R. China.

[b]Laboratory of Nanomedicine, School of Basic Medical Science, Henan University, Kaifeng 475004, China

[§]These authors contributed equally to this work.

[*]Dr. Wenkai Zhang, E-mail: zhangwenkai@henu.edu.cn

[*]Prof. Xianrui Meng, E-mail: mengxianrui@henu.edu.cn

[*]Prof. Xiaomin Fang, E-mail: xmfang@henu.edu.cn

Monitoring the growth of Ag NPs by LSPR spectra

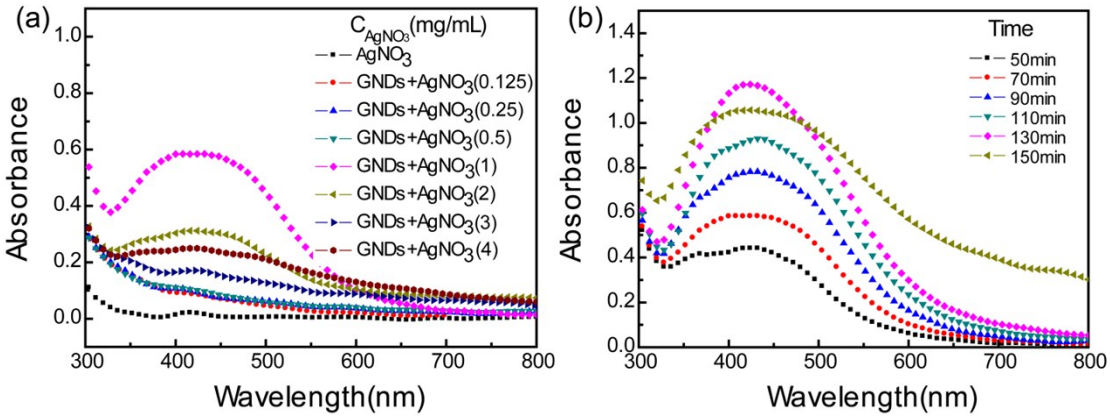

Figure S1 LSPR spectra of GND-supported Ag NPs as a function of precursor $AgNO_3$ concentration (a) and irradiation time (b). The intensity of LSPR peak increases but show little shift with the irradiation time, indicating the increasing number of Ag NPs during photoreduction, instead of particle size.

The effect of GND template on the loaded Ag NPs

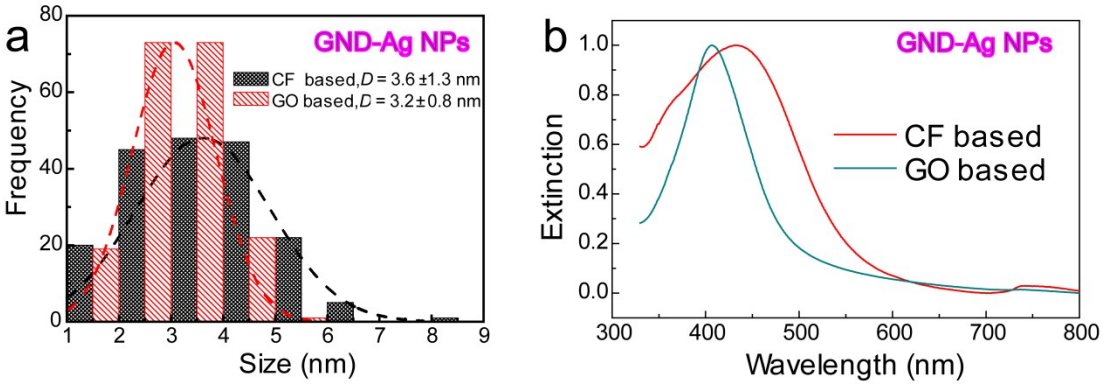

Figure S2 (a) The TEM size histogram of GND-Ag NPs. GNDs are synthesized by using carbon fiber (black) and GO (red) as starting materials. The mean values and standard deviations are shown inset. (b) LSPR spectra of GND-Ag NP solution. GND types: carbon fiber based (red); GO (cyan) based.

Estimation of surface density of deposited GND-Ag NPs

A direct method for calculating the surface concentration, Γ (particles·cm^{-2}), is to measure the number of GND-Ag NPs (N) present on a quartz substrate of known surface area (SA). We assume the GND-Ag NPs form a tightly packed well-ordered monolayer on quartz substrate, and then the surface density is defined as:

$$\Gamma\left(particles \cdot cm^{-2}\right) = \frac{N(particles)}{SA(cm^2)} \tag{1}$$

with the substrate surface area, SA, equal to 4.909 cm^2 (2.5 cm diameter quartz). In addition, the measurable mass of deposited GNDs-Ag NPs, is considered as the product of the mass of single particle, m_0, and the particle numbers, N:

$$m = N \cdot m_0 \tag{2}$$

The GNDs-Ag nanoparticle is briefly treated as quasi-sphere with a radius (r_{Ag}) of 1.6 nm and specific gravity (ρ_{Ag}) of 10.5 g·cm^{-3}. Then the eq(2) can be written as:

$$m = N \cdot \rho_{Ag} \cdot \frac{4}{3}\pi r_{Ag}^{3} = \gamma_i \cdot V \tag{3}$$

where γ_i is the mass concentration and the V is the pipetted volume of the GND-Ag NP solution. During the casting process, the γ_i in the range of 4-50 μg·mL^{-1}, and the V is 300 μL. Finally, the surface density can be determined as:

$$\Gamma\left(particles \cdot nm^{-2}\right) = 8.893 \times 10^{10}\gamma_i \tag{4}$$

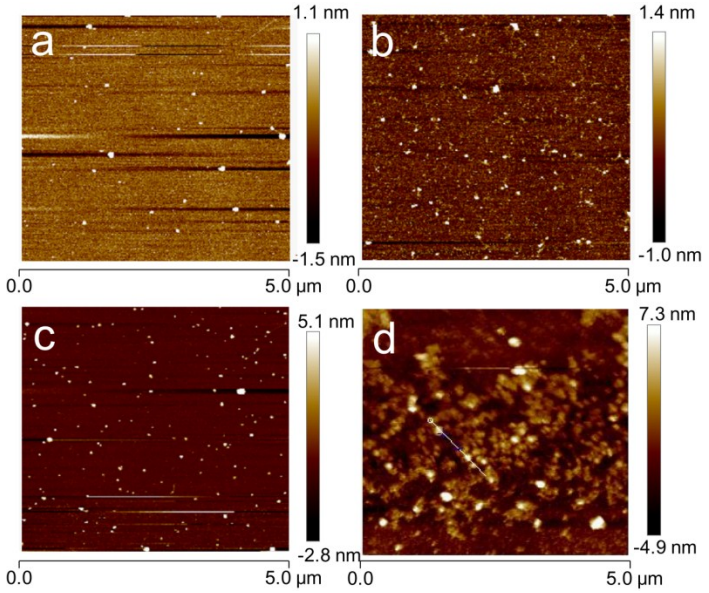

Figure S3 The AFM images of GND-Ag NPs on quartz when casting from increasing concentration of solution. (a) 4 μg/mL; (b) 8 μg/mL; (c) 12 μg/mL; (d) 50 μg/mL.

PL quenching of GNDs by the loaded Ag NPs

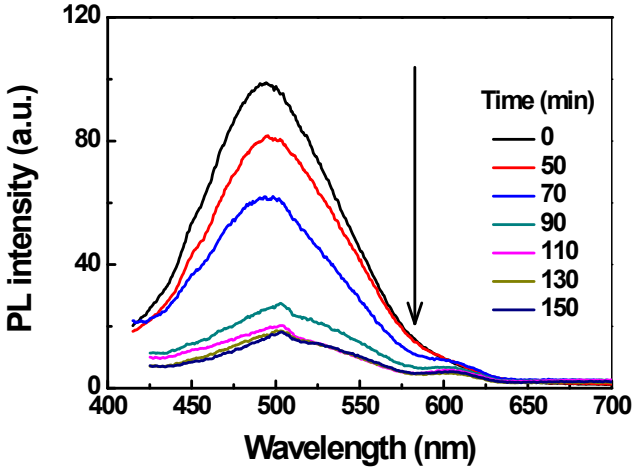

Figure S4 PL spectra of the GNDs and $AgNO_3$ mixture at increasing irradiating time, indicating the growing Ag loadings induce increasing PL quenching of the GNDs. The concentrations of GNDs and $AgNO_3$ solution are 0.1 mg/mL and 1 mg/mL, respectively. 254 nm UV lamp (8 W) was adopted.

Morphologies of spun CP films

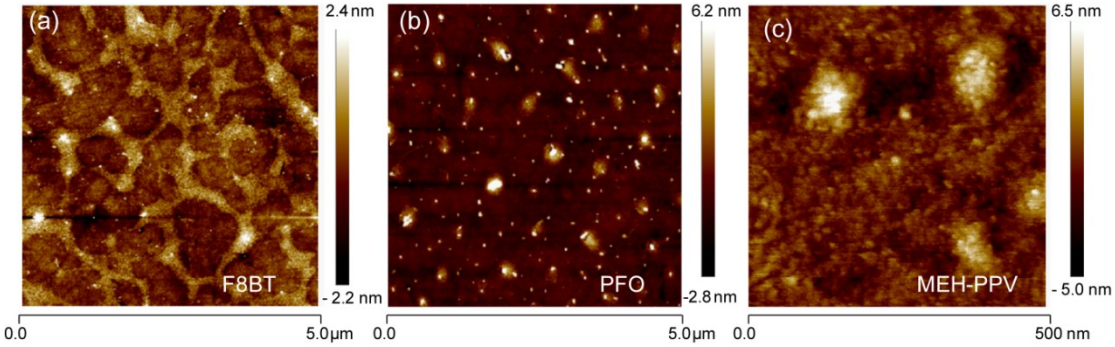

Figure S5 AFM images of the surface morphologies of spun CP films on quartz. (a) F8BT; (b) PFO; (c) MEH-PPV.

GND-Ag NP surface density dependent PL spectra

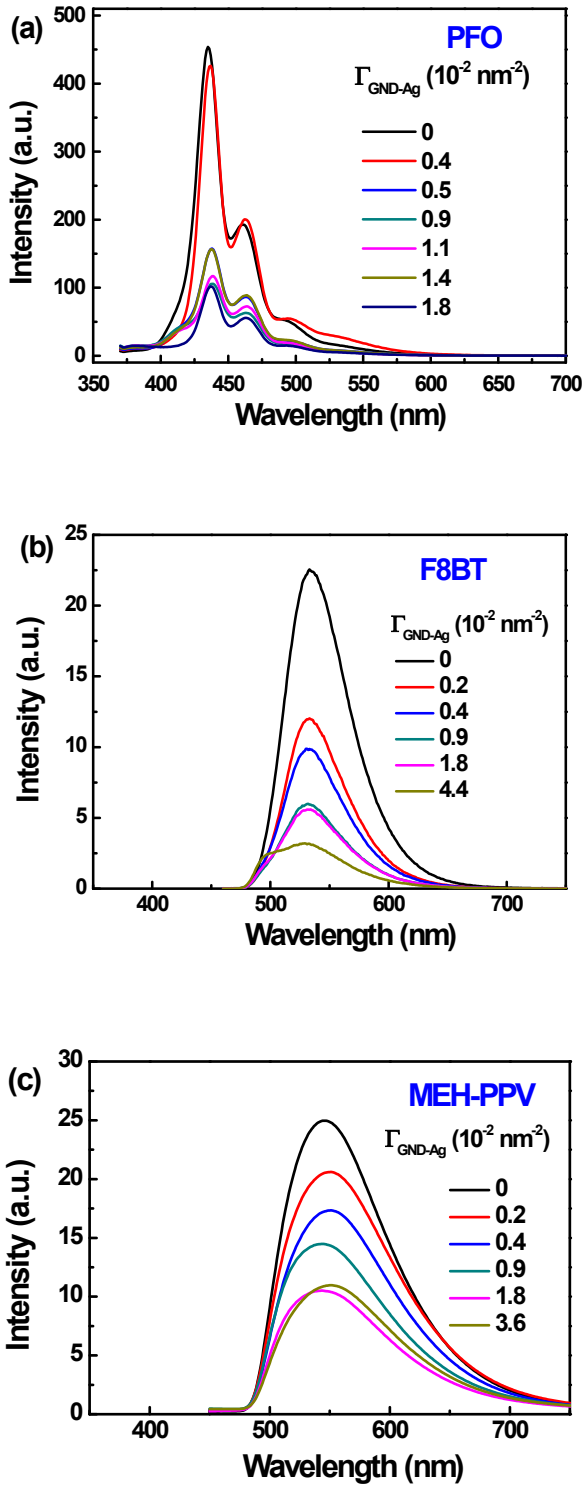

Figure S6 Steady PL spectra of CP films spun on top of GND-Ag NP monolayer with various surface densities of GND-Ag NPs, $\Gamma_{GND\text{-}Ag}$. (a) PFO, λ_{ex} = 350 nm; (b) F8BT, λ_{ex} = 420 nm; (c) MEH-PPV, λ_{ex} = 420 nm.

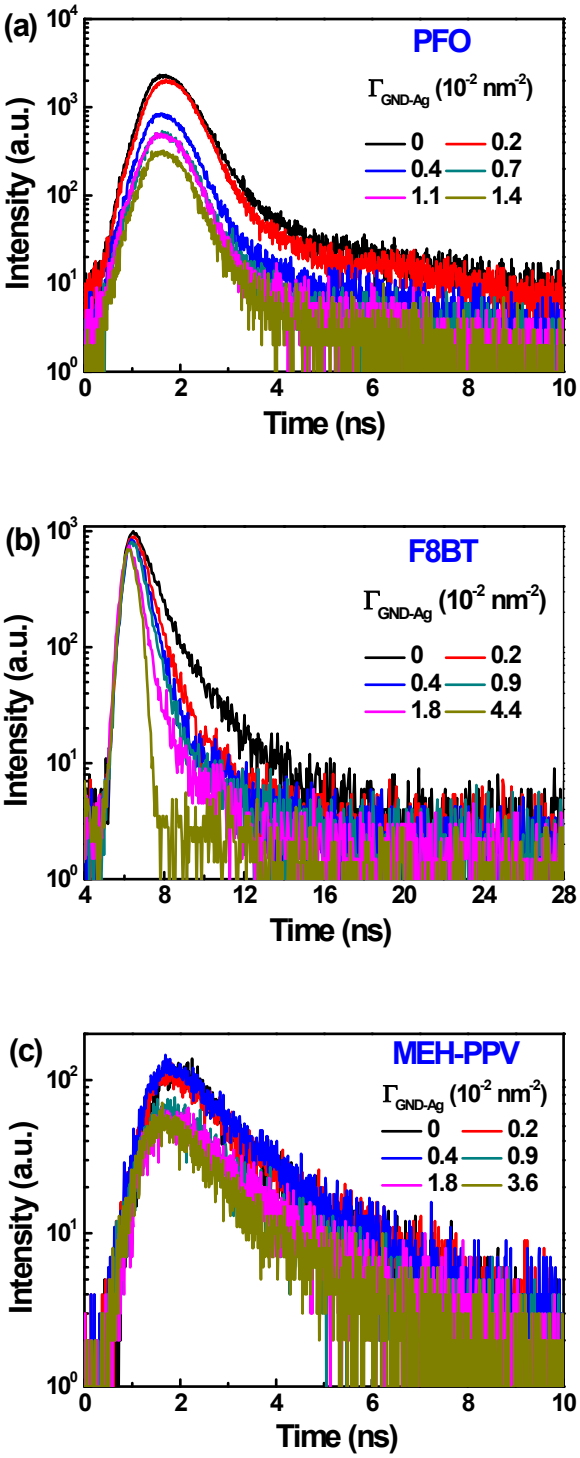

Figure S7 Transient PL decay curves of CP films spun on top of GND-Ag NP monolayer with various surface densities of GND-Ag NPs, Γ_{GND-Ag}. (a) PFO, λ_{em} = 450 nm; (b) F8BT, λ_{em} = 550 nm; (c) MEH-PPV, λ_{em} = 600 nm.

CP film thickness dependence of the PL lifetime

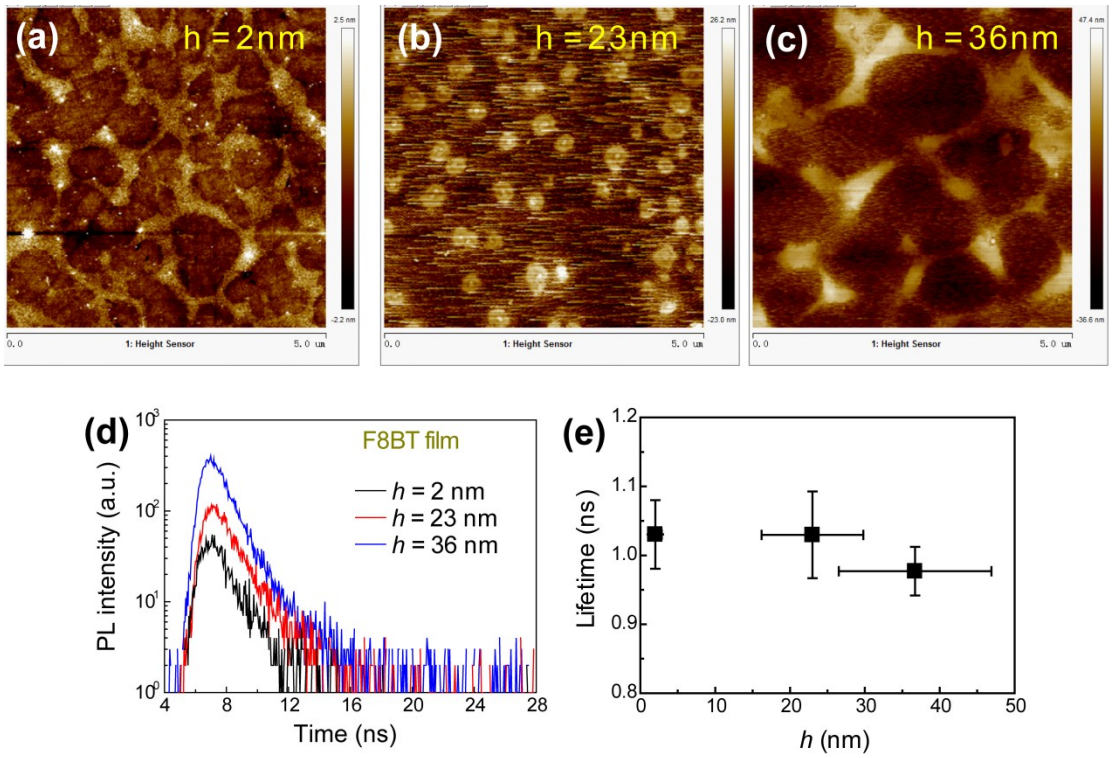

Figure S8 (a-c) AFM images of the surface morphologies of spun F8BT films with various thickness, *h*. (a) 2 nm; (b) 23 nm; (c) 36 nm. (d) Transient PL decay curves of F8BT films with various thicknesses. (e) PL lifetime of F8BT films as a function of film thickness.

Table S1 The CP film thickness dependence of PL lifetime.

	h (nm)	PL lifetime (ns)
PFO	3±0.6	0.58±0.06
	15±3.8	0.55±0.06
	39±9	0.52±0.03
F8BT	2±0.8	1.03±0.05
	23.0±6.79	1.03±0.06
	36±10.2	0.98±0.06
MEH-PPV	20±1.3	1.45±0.14
	25.8±5.3	1.11±0.04

Table S2 Quenching distances reported for various CP based energy transfer system.

Donor polymer	Quencher	Quenching distance[a] (nm)	Ref
PFO	PPV	6.3	[1]
PFO	hole	2.7	[2]
PFO	tetraphenylporphyrin	4.2	[3]
PFO	GND-Ag NPs	5.9-6.3	This work
F8BT	F8TBT	5.32	[4]
F8BT	MoO_3	4.5	[5]
F8BT	GND-Ag NPs	2.5-3.2	This work
MEH-PPV	C_{61}PCBM	3.4	[6]
MEH-PPV	GND-Ag NPs	8.3-11.6	This work

[a]The quenching distance corresponds to the Förster radius (R_0) calculated from FRET theory when the non-metal quencher is used, while corresponds to the characteristic distance d_0 calculated from PRET theory using GND-Ag NPs as quencher in this work.

Measurements of $(PDDA/PSS)_n$/PDDA spacer thickness

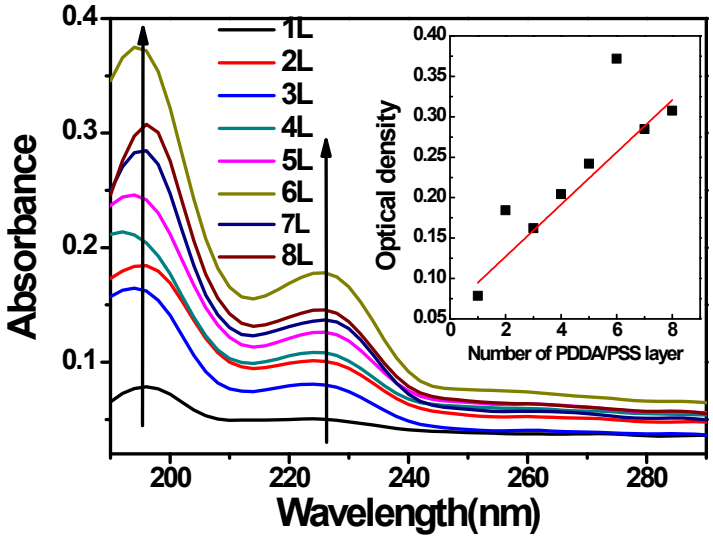

Figure S9 Absorption spectra of assembled $(PDDA/PSS)_n$/PDDA layer with the integer n = 0 to 8. Inset shows the optical density as a function of the number of PDDA/PSS layer monitored at 225 nm.

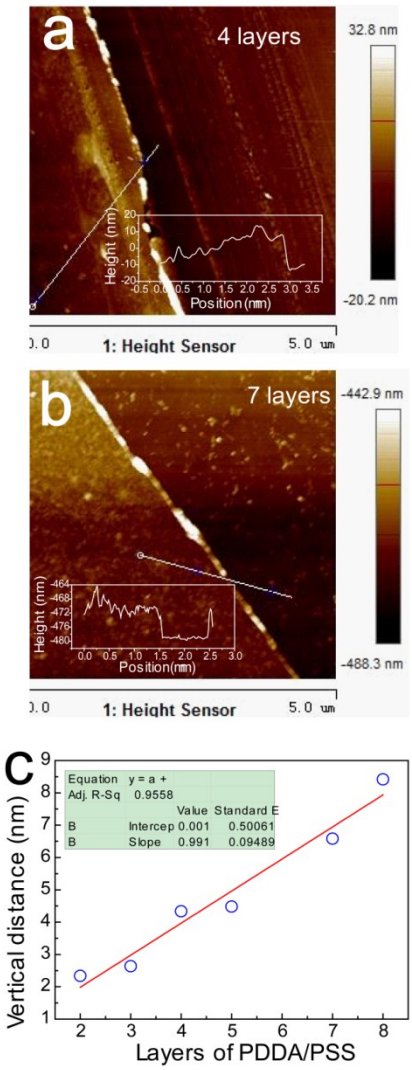

Figure S10 The thickness of $(PDDA/PSS)_n/PDDA$ layer with the n = 0 to 8 was measured using an AFM. The film was scratched with a wood stick and the step height along several scratches was measured. AFM images of scratch layer border with n = 4 (a) and 7 (b) show above. (c) The measured thickness of self-assembled film as a function of number of layers. The red line represents the linear fit equation $y = 0.99x$, indicating a self-assembled layer is about 1 nm.

Absorption spectra of the bilayer structure

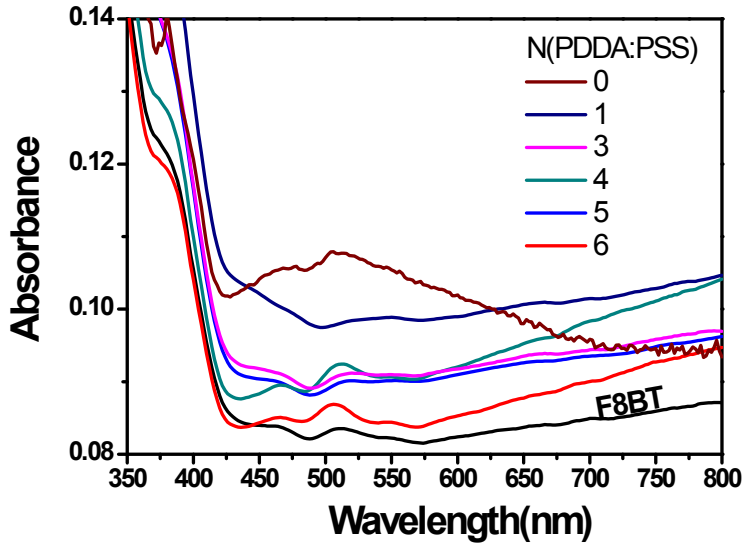

Figure S11 Absorption spectra of the bilayer structure of GND-Ag NPs/[(PDDA/PSS)$_n$/PDDA]/F8BT with the integer n = 0 to 6, where the Γ-value was set to be 4.4×10^{-2} nm^{-2} and the h_{CP} was 2 nm.

Spacer thickness dependent transient PL spectra

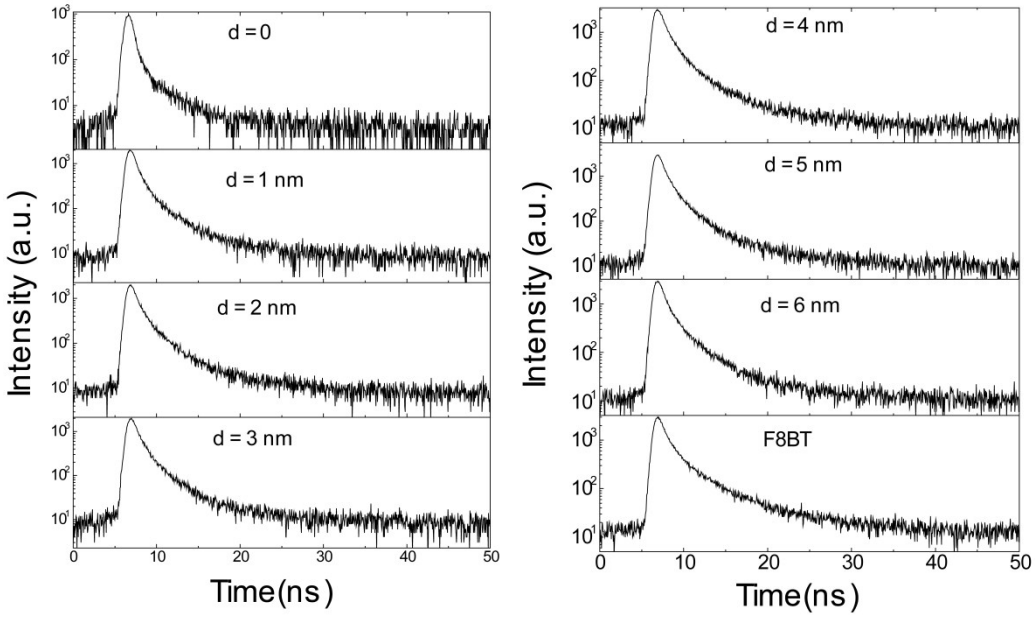

Figure S12 Transient PL decay curves of the bilayer structure of GND-Ag NPs/[(PDDA/PSS)$_n$/PDDA]/F8BT with the spacer thickness ranging from 0 to 6 nm, where the Γ-value was set to be 4.4×10^{-2} nm^{-2} and the h was 2 nm.

.

Photoelectrochemical study

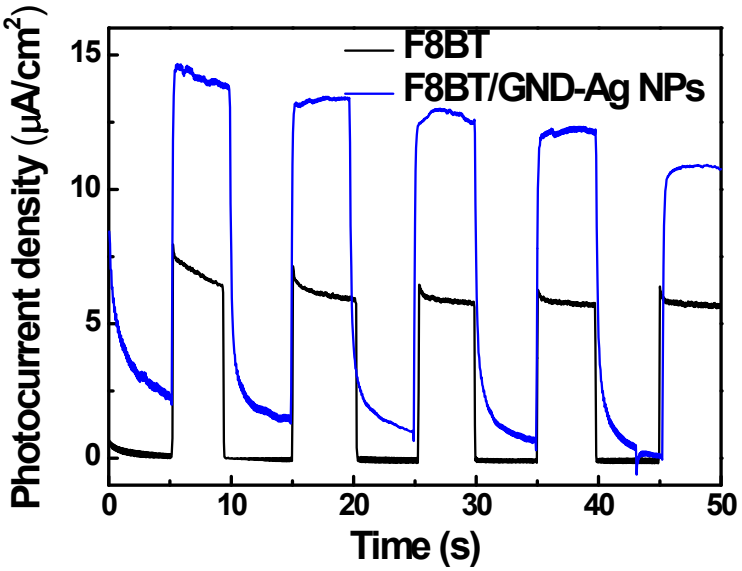

Figure S13 Photocurrent density versus time curves of F8BT films on ITO (black) and GND-Ag NPs (blue) photoanodes in sat. KCl as reference electrode, Pt wire as counter electrode and the prepared films with an active area ca. 0.12 cm^2 as working electrode. Light source: 300 W Xe lamp (100 $mW \cdot cm^{-2}$); Scanning rate: 20 $mV \cdot s^{-1}$.

References:

1. Muhammad-Umair Hassaan, Yee-Chen Liu, Kamran-Ul Hasan, Mohsin Rafique, Ali-K Yetisen, Haider Butt, Richard-Henry Friend, Highly Efficient Energy Transfer in Light Emissive Poly(9,9-dioctylfluorene) and Poly(p-phenylenevinylene) Blend System. ***ACS Photonics***, 2017, 5: 607-613.
2. Francisco Montilla, Arvydas Ruseckas, Ifor-D-W Samuel, Exciton‑Polaron Interactions in Polyfluorene Films with β-Phase. ***The Journal of Physical Chemistry C***, 2018, 122: 9766-9772.
3. G Cerullo, S Stagira, M Zavelani-Rossi, S De Silvestri, T Virgili, D-G Lidzey, D-D-C Bradley, Ultrafast Förster transfer dynamics in tetraphenylporphyrin doped poly(9,9-dioctylfluorene). ***Chemical Physics Letters***, 2001, 335: 27-33.
4. Bo-Ram Lee, Wonho Lee, Thanh-Luan Nguyen, Ji-Sun Park, Ji-Seon Kim, Jin-Young Kim, Han-Young Woo, Myoung-Hoon Song, Highly Efficient Red-Emitting Hybrid Polymer Light-Emitting Diodes via Förster Resonance Energy Transfer Based on Homogeneous Polymer Blends with the Same Polyfluorene Backbone. ***ACS Applied Materials & Interfaces***, 2013, 5: 5690-5695.
5. Aravindh Kumar, Amrita Dey, Anjali Dhir, Dinesh Kabra, Quantitative estimation of exciton quenching strength at interface of charge injection layers and organic semiconductor. ***Organic Electronics***, 2017, 42: 28-33.
6. Alexander-J Ward, Arvydas Ruseckas, Ifor-D-W Samuel, A Shift from Diffusion Assisted to Energy Transfer Controlled Fluorescence Quenching in Polymer−Fullerene Photovoltaic Blends. ***The Journal of Physical Chemistry C***, 2012, 116: 23931-23937.